EurJIC
European Journal of Inorganic Chemistry

Full Papers
doi.org/10.1002/ejic.202100364

Chemistry Europe
European Chemical Societies Publishing

Utilization of Rhenium(I) Polypyridine Complexes Featuring a Dinitrophenylsulfonamide Moiety as Biothiol-Selective Phosphorogenic Bioimaging Reagents and Photocytotoxic Agents

Guang-Xi Xu,[a] Lawrence Cho-Cheung Lee,[a] Cyrus Wing-Ching Kwok,[a] Peter Kam-Keung Leung,[a] Jing-Hui Zhu,[a] and Kenneth Kam-Wing Lo*[a, b, c]

We report herein a series of rhenium(I) polypyridine complexes featuring a 2,4-dinitrophenylsulfonamide (DNPS) unit as phosphorogenic bioimaging reagents and photocytotoxic agents. The biothiol-selective rhenium(I) polypyridine complexes [Re(N^N)(CO)$_3$(py-DNPS)](CF$_3$SO$_3$) (py-DNPS = 3-((2,4-dinitrophenylsulfonyl)aminomethyl)pyridine) and their DNPS-free counterparts [Re(N^N)(CO)$_3$(pyridine)](CF$_3$SO$_3$) were synthesized and characterized. Upon photoexcitation, the DNPS complexes exhibited very weak luminescence as a result of photoinduced electron transfer (PET) from the excited rhenium(I) diimine moiety to the DNPS quenching unit. However, upon treatment with glutathione (GSH), the DNPS moiety was removed, resulting in emission enhancement of the solutions (I/I_o = 12.6–22.2). After reaction of the DNPS complexes with GSH in living cells, intense intracellular emission and potent photocytotoxicity were both observed. Additionally, the modification of the diimine ligand with a tosylamide unit conferred on the complexes an endoplasmic reticulum (ER)-targeting ability, which can be exploited for selective bioimaging and photocytotoxic applications.

Introduction

As the most common biothiol in cells, glutathione (GSH) plays a crucial role in biological processes such as xenobiotic metabolism, intracellular redox status regulation, and cell differentiation.[1] Due to the high reactivity of the sulfhydryl group of GSH, significant effort has been devoted to the design of GSH-responsive bioimaging probes based on different reaction mechanisms including nucleophilic reaction,[2] Michael addition,[3] and disulfide cleavage.[4] The development of GSH-activatable photosensitizers for photodynamic therapy (PDT) has also attracted considerable attention in the past few decades.[5] PDT is an attractive modality for cancer therapy due to its non-invasive nature and minimal adverse effects.[6] However, the damage to ambient normal tissues caused by the photosensitizers through the generation of cytotoxic singlet oxygen ($^1O_2$) cannot be totally avoided due to a lack of cancer selectivity.[7] Thus, the introduction of a GSH-responsive unit to the photosensitizers is expected to modulate their $^1O_2$ generation efficiency and allow them to selectively produce cytotoxic $^1O_2$ in cancer cells, which are known to display an elevated GSH level compared to normal cells.[8]

Endoplasmic reticulum (ER) is the largest cellular organelle in eukaryotic cells that is responsible for the synthesis, folding, and post-translational modification of intracellular proteins.[9a,b] It is also involved in the storage of Ca^{2+} ions and lipid biosynthesis.[9c,d] Perturbation of the protein-folding ability of ER causes dysregulation of ER functions and leads to ER stress, which is known to be associated with various pathological conditions including heart disease, stroke, and neurodegenerative diseases.[10] Notably, GSH and its oxidized form (GSSG) are an important thiol redox couple for the regulation of redox homeostasis in the ER.[11] On the basis of previous ER-targeting probes,[12,13] real-time imaging of ER through a GSH-activation pathway is anticipated to be a useful strategy to understand its physiological functions.

In view of the rich photophysical properties and tunable cellular uptake behavior of transition metal complexes,[14] iridium(III) and ruthenium(II) complexes have been developed as GSH-responsive probes for bioimaging[15] and photosensitizers for PDT.[16] However, to the best of our knowledge, GSH-sensitive phosphorogenic rhenium(I) polypyridine complexes have been rarely examined.[17] We envisage that the incorporation of a GSH-responsive 2,4-dinitrophenylsulfonamide (DNPS) unit into rhenium(I) polypyridine complexes will afford a new generation of GSH-responsive agents for biological applications. Herein, we report the synthesis and characterization of a series of rhenium(I) polypyridine complexes

[a] G.-X. Xu, Dr. L. C.-C. Lee, C. W.-C. Kwok, P. K.-K. Leung, J.-H. Zhu, Prof. K. K.-W. Lo
Department of Chemistry
City University of Hong Kong
Tat Chee Avenue, Kowloon, Hong Kong, P. R. China
E-mail: bhkenlo@cityu.edu.hk
[b] Prof. K. K.-W. Lo
State Key Laboratory of Terahertz and Millimeter Waves
City University of Hong Kong
Tat Chee Avenue, Kowloon, Hong Kong, P. R. China
[c] Prof. K. K.-W. Lo
Center of Functional Photonics
City University of Hong Kong
Tat Chee Avenue, Kowloon, Hong Kong, P. R. China

Supporting information for this article is available on the WWW under https://doi.org/10.1002/ejic.202100364

Part of the joint "Metals in Medicine" Special Collection with ChemMedChem.

containing a DNPS moiety [Re(N^N)(CO)$_3$(py-DNPS)](CF$_3$SO$_3$) (py-DNPS = 3-((2,4-dinitrophenylsulfonyl)aminomethyl)pyridine; N^N = 4-*N*-((*p*-toluenesulfonylamino)ethyl)aminomethyl-4′-methyl-2,2′-bipyridine (bpy-tosylamide) (**1a**), 3,4,7,8-tetramethyl-1,10-phenanthroline (Me$_4$-phen) (**2a**), 4,7-diphenyl-1,10-phenanthroline (Ph$_2$-phen) (**3a**), 1,10-phenanthroline (phen) (**4a**)) and their DNPS-free counterparts [Re(N^N)(CO)$_3$(pyridine)](CF$_3$SO$_3$) (N^N = bpy-tosylamide (**1b**), Me$_4$-phen (**2b**), Ph$_2$-phen (**3b**), phen (**4b**)) (Figure 1). The design of complexes **1a**–**4a** involved the modification of rhenium(I) polypyridine complexes with DNPS as a thiol-sensitive emission quenching moiety. The complexes are expected to show very weak emission due to efficient photoinduced electron transfer (PET) from the excited rhenium(I) polypyridine unit to the DNPS moiety. We anticipate that upon reaction with GSH, the DNPS unit will be removed from the complexes, leading to substantially increased emission intensities and lifetimes and enhanced $^1O_2$ generation efficiency. Since the tosylamide unit is known to specifically bind to ATP-sensitive K^+ channels in the ER membrane, complexes **1a** and **1b** containing a bpy-tosylamide unit are expected to display ER-targeting capability.

Results and Discussion

Synthesis

Rhenium(I) polypyridine complexes were chosen as the model luminophore in this study due to their interesting photophysical characteristics and tunable cellular uptake and localization properties.[18] The DNPS moiety was introduced to the pyridine ligand as it can be cleaved by GSH, which will allow modulation of the emission properties and photoinduced $^1O_2$ generation of the complexes. The synthetic procedure of the ligand py-DNPS involved the reaction of 3-(aminomethyl)pyridine with 2,4-dinitrophenylsulfonyl chloride in dry THF. A tosylamide group was introduced as an ER-targeting unit to the diimine ligand of complexes **1a** and **1b**. The ligand bpy-tosylamide was prepared by reductive amination of 4-formyl-4′-methyl-2,2′-bipyridine (bpy-CHO) with *N*-(2-aminoethyl)-4-methylbenzenesulfonamide. Reaction of the precursor [Re(N^N)(CO)$_3$(CH$_3$CN)](CF$_3$SO$_3$) with py-DNPS in refluxing THF led to the formation of complexes **1a**–**4a**. The DNPS-free complexes **1b**–**4b** were also prepared for comparison studies. All the complexes were characterized by ESI-MS, ^{1}H and ^{13}C NMR, IR spectroscopy, and gave satisfactory elemental analysis.

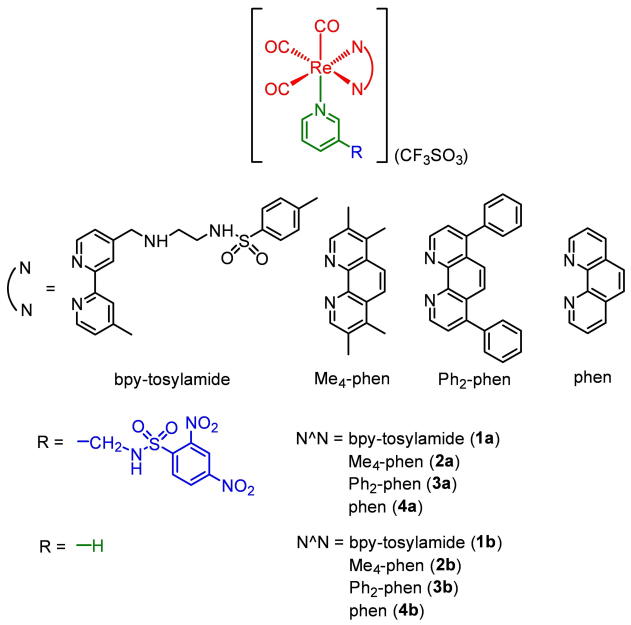

Figure 1. Structures of the rhenium(I) polypyridine complexes.

Photophysical properties

The electronic absorption data of the ligand py-DNPS and the rhenium(I) polypyridine complexes at 298 K are presented in Table S1 and the electronic absorption spectra are shown in Figure S1. Complexes **1a**–**4a** showed intense spin-allowed intraligand (^{1}IL) ($\pi\rightarrow\pi^*$) (N^N and pyridine) absorption at ≈250–320 nm (ε on the order of 10^4 dm^3 mol^{-1} cm^{-1}) and weaker spin-allowed metal-to-ligand charge-transfer (^{1}MLCT) ($d\pi(Re)\rightarrow\pi^*(N^N)$) absorption bands/shoulders at ≈320–390 nm, which is in accordance with previously reported rhenium(I) complexes.[18d,e,19] Notably, the DNPS complexes **1a**–**4a** exhibited stronger absorption in the UV region than their DNPS-free counterparts **1b**–**4b** due to the DNPS unit.

Upon irradiation, the rhenium(I) polypyridine complexes showed green to yellow emission in degassed solutions under ambient conditions and in low-temperature alcohol glass. The photophysical data are listed in Table 1. Importantly, complexes **1a**–**4a** revealed much weaker emission intensity (Φ_{em} = 0.003–

Table 1. Photophysical data of the rhenium(I) polypyridine complexes.

Complex	Medium (*T* [K])	λ_{em} [nm]	τ_o [μs]	Φ_{em}
1a	CH_2Cl_2 (298)	537	0.19	0.007
	CH_3CN (298)	550	0.12	0.003
	Glass[a] (77)	490	4.31	
1b	CH_2Cl_2 (298)	535	0.69	0.18
	CH_3CN (298)	557	0.24	0.04
	Glass[a] (77)	492	4.36	
2a	CH_2Cl_2 (298)	515	0.12	0.015
	CH_3CN (298)	516	< 0.1	0.004
	Glass[a] (77)	465 (max), 498, 535	34.73	
2b[17b]	CH_2Cl_2 (298)	490 sh, 510	11.88	0.57
	CH_3CN (298)	485 sh, 515	8.70	0.28
	Glass[a] (77)	466 (max), 499, 535	50.57	
3a	CH_2Cl_2 (298)	541	0.18	0.017
	CH_3CN (298)	551	< 0.1	0.008
	Glass[a] (77)	504, 530 sh	22.69	
3b[17b]	CH_2Cl_2 (298)	542	9.08	0.46
	CH_3CN (298)	558	4.04	0.13
	Glass[a] (77)	508	19.85	
4a	CH_2Cl_2 (298)	531	0.21	0.043
	CH_3CN (298)	546	< 0.1	0.009
	Glass[a] (77)	492	11.29	
4b	CH_2Cl_2 (298)	531	2.79	0.33
	CH_3CN (298)	546	1.60	0.18
	Glass[a] (77)	497	10.19	

[a] EtOH/MeOH (4:1, *v*/*v*).

0.043) compared with their DNPS-free counterparts **1b**–**4b** (Φ_{em} = 0.04–0.57) in solutions at 298 K, as a result of emission quenching by the appended DNPS moiety. Complexes **1a**,**b**, **3a**,**b**, and **4a**,**b** displayed a broad emission band that showed a red-shift upon changing the solvent from less polar CH_2Cl_2 to more polar CH_3CN, which is a typical feature of triplet metal-to-ligand charge-transfer (^{3}MLCT) (dπ(Re)→π*(N^N)) emission.[18d,e] In contrast, the Me_4-phen complexes **2a**,**b** exhibited a structured emission band with very long emission lifetimes (34.73 and 50.57 μs, respectively) in alcoholic glass at 77 K, indicative of the involvement of triplet intraligand (^{3}IL) (π→π*) (Me_4-phen) character in the ^{3}MLCT (dπ(Re)→π*(Me_4-phen)) emissive state.[18d,19]

Electrochemical properties

The electrochemical properties of the rhenium(I) polypyridine complexes were investigated by cyclic voltammetry and the data are listed in Table 2. With reference to the previous electrochemical studies of related rhenium(I) polypyridine complexes,[20] the quasi-reversible couples of the complexes at +1.54 to +1.69 V and −1.17 to −1.41 V versus SCE were assigned to the metal-centered rhenium(II)/(I) couple and the reduction of diimine ligands, respectively. The additional quasi-reversible couples of complexes **1a**–**4a** at −0.75 to −0.81 V were attributed to the reduction of the py-DNPS ligand, as a similar reduction couple was observed for the uncoordinated py-DNPS ligand at a slightly more cathodic potential (−0.88 V). On the basis of the low-temperature emission energy (E^{00} = 2.46–2.67 eV, Table 1) and the redox potentials ($E^{\circ}[Re^{2+/+}]$) of complexes **1a**–**4a** (+1.61 to +1.69 V), the excited-state redox potentials ($E^{\circ}[Re^{2+/+*}]$) were determined to range from −0.85 to −1.07 V versus SCE. These values are more negative than the reduction potential of the coordinated py-DNPS ligand (−0.75 to −0.81 V), demonstrating that PET from the excited rhenium(I) polypyridine unit to the appended DNPS moiety is thermodynamically favorable (ΔG° = −0.06 to −0.31 eV), which is believed to contribute to efficient emission quenching.

Table 2. Electrochemical data of the rhenium(I) polypyridine complexes and the free ligand py-DNPS.[a]

Compound	Oxidation, $E_{1/2}$ [V]	Reduction, $E_{1/2}$ or E_c [V]
1a	+1.69[b]	−0.78,[b] −1.31,[b] −1.64,[b] −1.93[b]
1b	+1.64[b]	−1.22,[c] −1.61, −1.85[b]
2a	+1.61[b]	−0.75,[b] −1.41,[b] −1.66,[b] −1.87[b]
2b	+1.54[b]	−1.30,[b] −1.75, −1.98[b]
3a	+1.62[b]	−0.79,[b] −1.21,[b] −1.58,[b] −1.89[b]
3b	+1.61[b]	−1.23,[c] −1.5, −1.71[b]
4a	+1.66[b]	−0.81,[b] −1.17,[b] −1.45[b]
4b	+1.58[b]	−1.16,[c] −1.41
py-DNPS		−0.88, −1.39[b]

[a] In CH_3CN (0.1 M TBAP) at 298 K, glassy carbon electrode, sweep rate = 100 mV s^{-1}, all potentials are versus SCE. [b] Quasi-reversible couples. [c] Irreversible waves.

Phosphorogenic responses toward GSH

As the electron-withdrawing DNPS moiety is readily cleaved upon reaction with GSH through thiol-induced elimination,[15c] the sensitivity of complexes **1a**–**4a** toward GSH was studied. After incubation with GSH (1 mM) in aerated aqueous buffer at 298 K for 12 h, solutions of complexes **1a**–**4a** showed significant emission enhancement with extended emission lifetimes (I/I_o = 12.6–22.2, τ = 0.13–1.20 μs) (Table 3 and Figure 2). These photophysical changes were ascribed to thiol-induced removal of the quenching DNPS moiety (Scheme 1), resulting in the formation of the strongly emissive aminomethylpyridine complexes **1aP**–**4aP** (Table S2). As shown in Figure 3, incubation of complex **1a** with GSH led to a drop of absorption at 260 nm and an increase at 360 nm with sharp isosbestic points at 260 and 300 nm. This indicates the clean conversion of the complex into its aminomethylpyridine counterpart **1aP**, which was confirmed by a peak at m/z = 776 in the ESI-mass spectrum of the CH_2Cl_2 extract of the reaction mixture (Figure S2). Time-dependent emission enhancement studies indicated that after incubation of complex **1a** (10 μM) with GSH (1 mM), the emission intensity of the solutions increased gradually and equilibrated in < 30 min (Figure 4). Since the emission intensity of a bioprobe should be independent on pH, at least in the physiological range,[21] the effect of pH on the response of complex **1a** toward GSH was evaluated. Figure S3 illustrates that the emission intensities of both complex **1a** and its aminomethylpyridine counterpart **1aP** remained stable in the pH range of 6–9, indicating that complex **1a** can give reliable emission response toward GSH at physiological pH (≈7.0–8.0).

The selectivity of complex **1a** toward GSH was examined by emission measurements. The emission changes of complex **1a**

Table 3. Emission enhancement factors and lifetimes of a mixture of complexes **1a**–**4a** (10 μM) and GSH (1 mM) in aerated potassium phosphate buffer (50 mM, pH 7.4)/MeOH (9:1, *v*/*v*) upon incubation at 298 K for 12 h.[a]

Complex	I/I_o[b]	τ [μs]
1a	18.2	0.13
2a	12.6	1.20
3a	12.9	1.10
4a	22.2	0.59

[a] In the absence of GSH, the emission lifetimes of the complexes could not be determined accurately. [b] I_o and I are the emission intensities of a solution of the complexes in the absence and presence of GSH (1 mM), respectively.

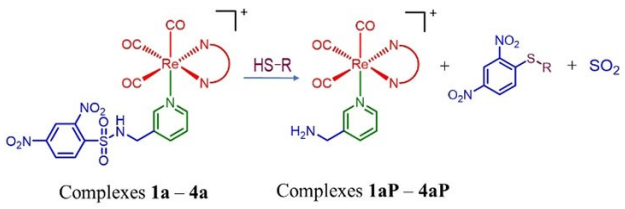

Scheme 1. Reaction of the rhenium(I) DNPS complexes **1a**–**4a** with a thiol (HS–R) yielding complexes **1aP**–**4aP**.

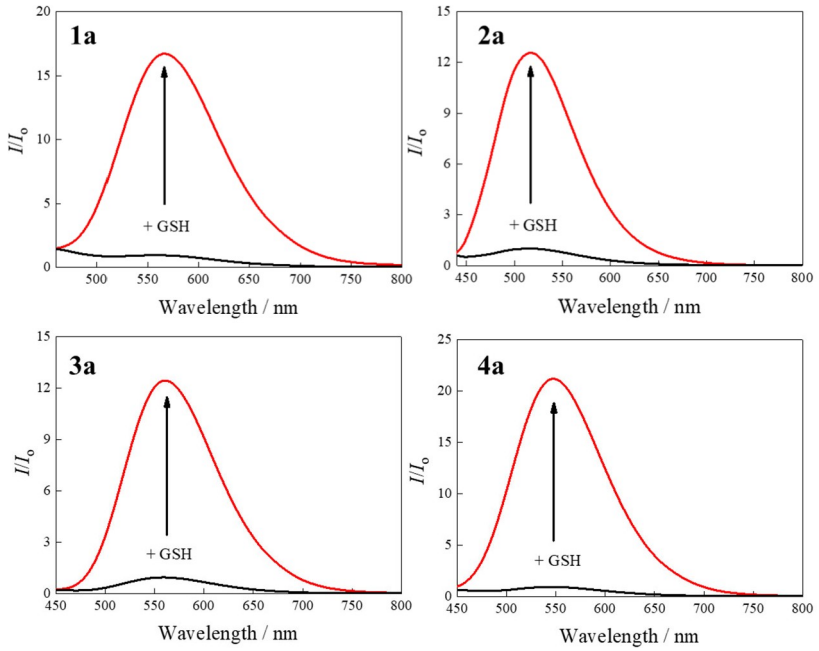

Figure 2. Emission spectra of complexes **1 a**–**4 a** (10 μM) in the absence (black) and presence (red) of GSH (1 mM) in aerated potassium phosphate buffer (50 mM, pH 7.4)/MeOH (9 : 1, *v*/*v*) upon incubation at 298 K for 12 h. Excitation wavelength = 355 nm.

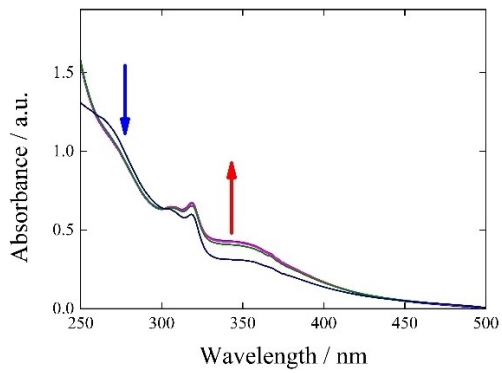

Figure 3. UV-Vis absorption spectral traces of a mixture of complex **1 a** (10 μM) and GSH (1 mM) in aerated potassium phosphate buffer (50 mM, pH 7.4)/MeOH (9 : 1, *v*/*v*) upon incubation at 298 K from 0 to 1 h.

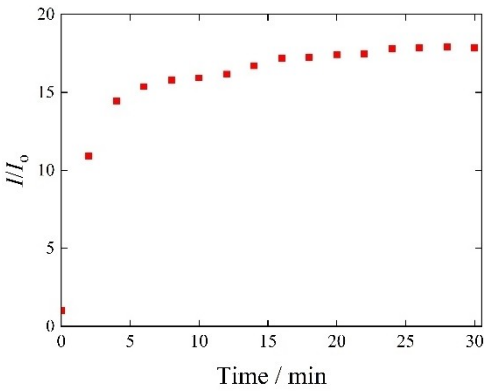

Figure 4. Time-dependent emission curve of complex **1 a** (10 μM) with GSH (1 mM) in aerated potassium phosphate buffer (50 mM, pH 7.4)/MeOH (9 : 1, *v*/*v*) at 298 K. Excitation wavelength = 355 nm.

(10 μM) upon incubation with a variety of biologically relevant molecules including amino acids, reactive oxygen species, and reactive nitrogen species (1 mM) are summarized in Figure 5. The emission of complex **1 a** only showed enhancement after treatment with GSH and cysteine (Cys) due to thiol-induced DNPS elimination. Since the concentration of GSH in an intracellular microenvironment (1–10 mM) is much higher than that of Cys (30–100 μM),[22] GSH is considered as the most reactive biothiol to the DNPS complexes, and the interference caused by Cys in cells is negligible.

The significant emission enhancement, good selectivity against competitive biomolecules, and pH-insensitive properties reveal that the rhenium(I) DNPS complexes are promising candidates as GSH-responsive reagents for cellular applications.

Cellular studies

The cellular uptake efficiencies, cytotoxicity, and bioimaging properties of the rhenium(I) polypyridine complexes were studied by inductively coupled plasma-mass spectrometry (ICP-MS), the 3-(4,5-dimethylthiazol-2-yl)-2,5-diphenyltetrazolium bromide (MTT) assay, and laser-scanning confocal microscopy (LSCM), respectively. Human cervix carcinoma (HeLa) cells were selected as the model cell line. As shown in Table 4, after incubation with the rhenium(I) polypyridine complexes (10 μM) for 2 h, an average HeLa cell contained 0.12–1.31 fmol of complexes. The cellular uptake efficiency of the complexes followed the orders: **3 a** > **2 a** > **1 a** ≈ **4 a** and **3 b** > **2 b** > **1 b** ≈ **4 b**, which is in line with the lipophilicity of the complexes due to

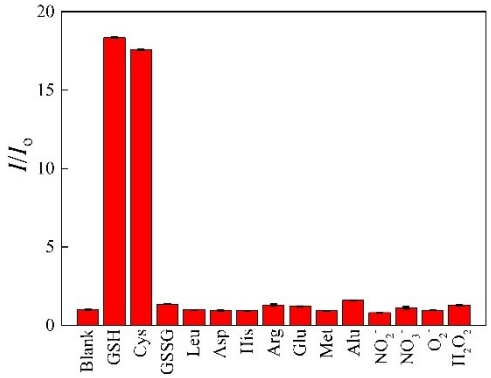

Figure 5. Emission enhancement factors (I/I_o) at 555 nm of complex **1a** (10 μM) in the presence of various reagents (1 mM) in aerated potassium phosphate buffer (50 mM, pH 7.4)/MeOH (9:1, *v/v*) upon incubation at 298 K for 12 h. Excitation wavelength = 355 nm.

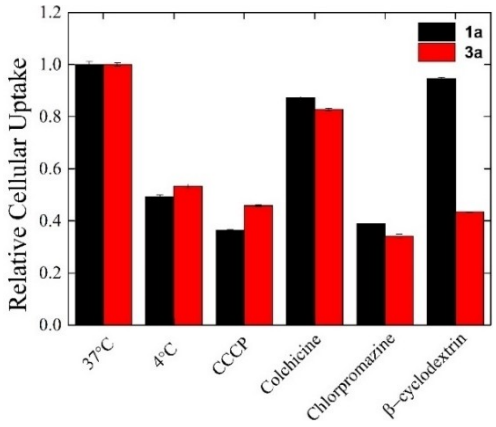

Figure 6. Relative cellular uptake of rhenium associated with an average HeLa cell after incubation with complexes **1a** (black) and **3a** (red) (10 μM) at 37 °C, 4 °C, and after preincubation with CCCP (20 μM), colchicine (12.5 μM), chlorpromazine (1 μM) and β-cyclodextrin (5 mM). Uptake values at 37 °C were taken as reference in each complex.

Table 4. Cellular uptake and cytotoxicity (IC_{50}, 24 h) of the rhenium(I) polypyridine complexes toward HeLa cells.

Complex	Amount of rhenium [fmol][a]	IC_{50} [μM]
1a	0.13 ± 0.01	33.7 ± 2.5
1b	0.12 ± 0.01	36.4 ± 0.8
2a	0.44 ± 0.02	12.7 ± 2.0
2b	0.55 ± 0.01	16.9 ± 1.0
3a	1.31 ± 0.01	6.50 ± 2.0
3b	0.99 ± 0.01	10.3 ± 0.5
4a	0.14 ± 0.01	32.9 ± 0.3
4b	0.20 ± 0.01	39.4 ± 1.3

[a] Amount of rhenium associated with an average HeLa cell upon incubation with the rhenium(I) polypyridine complexes (10 μM) at 37 °C for 2 h, as determined by ICP-MS.

the increasing hydrophobic nature of the diimine ligands: phen < Me_4-phen < Ph_2-phen. It is possible that the reduced cellular uptake efficiency of complexes **1a** and **1b** was caused by the bulky bpy-tosylamide. The uptake mechanism of complexes **1a** and **3a** was studied in more detail. Incubation of HeLa cells with complexes **1a** and **3a** at 4 °C led to lower uptake efficiency compared to the cells at 37 °C (Figure 6), indicating that the complexes were taken up by the cells via an energy-dependent pathway, which was further confirmed by the reduced uptake when the cells were treated with the metabolic inhibitor carbonyl cyanide 3-chlorophenylhydrazone (CCCP) (Figure 6).[23a] Next, the influence of different internalization pathway inhibitors on the uptake of complexes **1a** and **3a** was investigated. The changes in the cellular uptake efficiency of the complexes were negligible when HeLa cells were preincubated with the pinocytosis inhibitor colchicine (Figure 6).[23b] However, pretreatment of the cells with chlorpromazine,[23c] a typical clathrin-mediated endocytosis inhibitor, induced drastic reduction in the cellular uptake of the complexes (Figure 6), demonstrating that the complexes were internalized into the cells through clathrin-mediated endocytosis. Additionally, pretreatment with β-cyclodextrin,[23d] a caveolae-mediated endocytosis inhibitor, resulted in a decrease in the intracellular amount of rhenium for the cells incubated with complex **3a**, whereas the effect on complex **1a** was negligible (Figure 6). This result highlights that caveolae-mediated endocytosis is also important for the cellular uptake of complex **3a**. The cytotoxicity of all the rhenium(I) polypyridine complexes toward HeLa cells was presented as half-maximal inhibitory concentration (IC_{50}) values, which are summarized in Table 4. The results indicate that the orders of cytotoxicity of the complexes are **3a** > **2a** > **1a** ≈ **4a** and **3b** > **2b** > **1b** ≈ **4b**, which is in accordance with their cellular uptake efficiencies.

The phosphorogenic response of the rhenium(I) polypyridine complexes in live cells was investigated by regulating the intracellular concentration of GSH. After incubation with complex **1a** (10 μM) for 2 h, HeLa cells showed moderate emission (Figure 7), which is due to the reaction of the complex with intracellular GSH to give the emissive aminomethylpyridine complex **1aP**. Interestingly, much stronger intracellular emis-

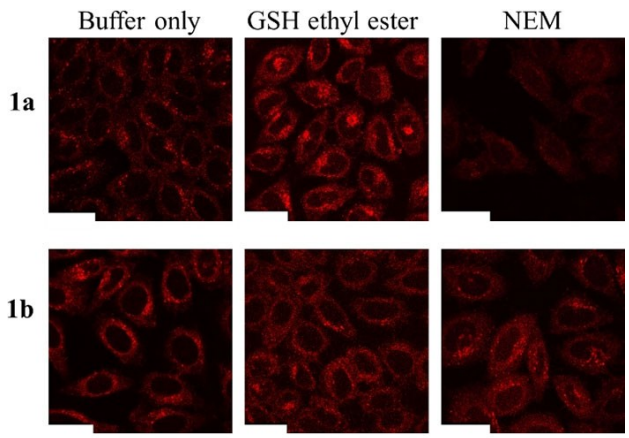

Figure 7. LSCM images of HeLa cells pretreated without or with GSH ethyl ester (1 mM, 37 °C, 2 h) or NEM (500 μM, 37 °C, 20 min), followed by washing with phosphate-buffered saline (PBS) and incubation with complexes **1a** and **1b** (10 μM, 37 °C, 2 h, λ_{ex} = 405 nm). Scale bar = 25 μm.

sion was observed when the cells had been pretreated with GSH ethyl ester (a source of exogenous GSH, 1 mM, 2 h) (Figure 7). However, when HeLa cells were pretreated with the thiol scavenger *N*-ethylmaleimide (NEM, 500 μM, 20 min), they showed extremely weak emission (Figure 7), which is a consequence of the reduced level of intracellular GSH. Importantly, cells stained with the DNPS-free complex **1b** (10 μM) displayed negligible changes in emission intensity in response to GSH ethyl ester or NEM pretreatment (Figure 7), which further supported that the observed intracellular emission was due to the specific reaction of the rhenium(I) DNPS complexes with GSH.

The ER-targeting ability of complexes **1a** and **1b**, both of which contain a bpy-tosylamide ligand, was evaluated by LSCM. HeLa cells treated with complex **1a** (10 μM, 2 h) revealed a strong emission intensity in the perinuclear region (Figure 8a). Co-staining experiments with ER-Tracker Green indicated that the complex was mainly accumulated in the ER, with a Pearson's colocalization correlation coefficient (PCCC) of 0.89 (Figure 8a). A similar result was also observed for complex **1b** (PCCC = 0.85) (Figure 8b). However, the tosylamide-free complexes **2a**–**4a** and **2b**–**4b** displayed significantly different intracellular distribution; for example, complex **3a** showed strong colocalization with MitoTracker Deep Red FM (PCCC = 0.93) (Figure 9), most likely due to its lipophilic and cationic character. Similar mitochondria-staining properties of related lipophilic and cationic transition metal complexes have been documented.[17,24]

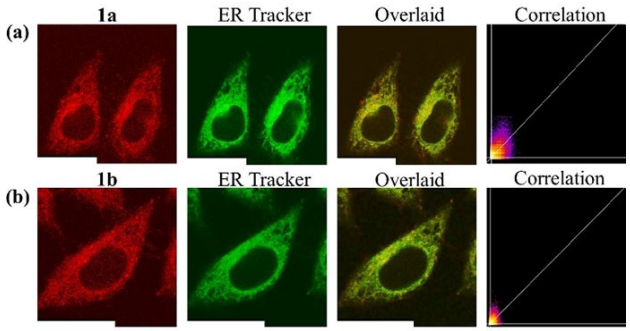

Figure 8. LSCM images of HeLa cells pretreated with complexes (a) **1a** and (b) **1b** (10 μM, 2 h, λ_{ex} = 405 nm) and then incubated with ER-Tracker Green (1 μM, 20 min, λ_{ex} = 488 nm, λ_{em} = 500–505 nm) at 37 °C. PCCC = 0.89 and 0.85, respectively. Scale bar = 25 μm.

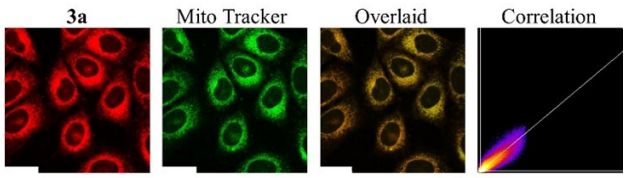

Figure 9. LSCM images of HeLa cells pretreated with complex **3a** (10 μM, 2 h, λ_{ex} = 405 nm) and then incubated with MitoTracker Deep Red FM (100 nM, 20 min, λ_{ex} = 635 nm, λ_{em} = 654–674 nm) at 37 °C. PCCC = 0.93. Scale bar = 25 μm.

It is well known that the $^1O_2$ generation efficiency of rhenium(I) polypyridine complexes is strongly associated with their long triplet-state lifetimes.[18a,25] For this reason, the exploration of the rhenium(I) DNPS complexes as controllable photosensitizers for PDT is of great interest. The $^1O_2$ generation quantum yields (Φ_Δ) of the rhenium(I) polypyridine complexes were determined in aerated DMSO using 1,3-diphenylisobenzofuran (DPBF) as a $^1O_2$ scavenger and the results are presented in Table 5. The Φ_Δ values of complexes **1b**–**4b** ranged from 0.20 to 0.75, which are much higher than those of complexes **1a**–**4a** (0.06–0.15). These results are attributable to the higher emission quantum yields and extended lifetimes of complexes **1b**–**4b**.[26]

Since the emission intensities and $^1O_2$ sensitization properties of complexes **1a**–**4a** rely on the removal of the DNPS unit upon reaction with GSH, the dependence of the photocytotoxicity of complex **3a** on the incubation time in the dark was studied. HeLa cells were treated with complex **3a** (1 μM) for 2 h in the dark and thoroughly washed with PBS. Then the cells were incubated in fresh medium for different periods (1–12 h) in the dark, followed by irradiation at 365 nm for 5 min (or incubation in the dark as a control), and further incubated in fresh medium for 24 h in the dark, before analyzed by the MTT assay. As shown in Figure 10, upon incubation in the dark for 12 h, complex **3a** displayed negligible cytotoxicity toward HeLa cells with cell viability > 95%. However, the cell viability decreased significantly from 82% (1 h) to 9% (12 h) upon irradiation (λ_{ex} = 365 nm, 5 min, light dose = 5 mW cm^{-2}) and the photocytotoxicity effect is most prominent from 1 to 3 h. The reduction of cell viability is attributable to the formation of the aminomethylpyridine complex **3aP** with efficient $^1O_2$ photosensitization; the presence of this product was confirmed by ESI-MS (Figure S4). Although complex **3a** was converted to **3aP** during this dark incubation in fresh medium, the intracellular rhenium concentration remained steady (at ≈1.3 fmol in an average HeLa cell). Thus, the variation of the photocytotoxicity of the complex at different incubation times should be a result of the formation of complex **3aP**. Summing up, all these results indicate that the cellular imaging capability and $^1O_2$ photosensitization properties of complex **3a** can be readily modulated by intracellular GSH, which is known to be elevated in level in cancerous cells.

Table 5. The $^1O_2$ generation quantum yields of the rhenium(I) polypyridine complexes in aerated DMSO at 298 K (λ_{ex} = 365 nm). DPBF was used as the $^1O_2$ scavenger and methylene blue as the standard (Φ_Δ = 0.52).

Complex	Φ_Δ
1a	0.06
1b	0.20
2a	0.09
2b	0.75
3a	0.15
3b	0.73
4a	0.07
4b	0.64

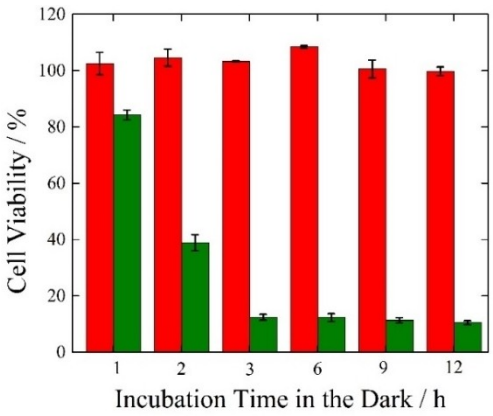

Figure 10. Viability of HeLa cells incubated with complex **3a** (1 μM) at 37 °C for 2 h in the dark, thoroughly washed with PBS and incubated in fresh medium for different periods (1, 2, 3, 6, 9, and 12 h) in the dark, followed by further incubation in the dark (red bars) or under irradiation at 365 nm for 5 min (light dose = 5 mW cm^{-2}) (green bars), and then incubated in fresh medium in the dark for 24 h, prior to analysis by the MTT assay. High viability (> 95 %) was observed upon irradiation of the cells for 5 min in the absence of the complex.

Conclusions

In this work, a series of rhenium(I) polypyridine complexes functionalized with a DNPS moiety was synthesized and characterized. Due to the efficient PET quenching by the DNPS unit, complexes **1a**–**4a** exhibited very weak emission after photoexcitation. However, upon incubation with GSH, strong emission enhancement of the solutions was observed. Additionally, the rhenium(I) DNPS complexes showed good reaction selectivity and pH-independent emission intensity. Cellular uptake experiments indicated that energy-dependent endocytosis is the main uptake pathway for the complexes. Upon activation by intracellular GSH, the rhenium(I) DNPS complexes displayed intriguing photophysical properties, including intense emission and $^1O_2$ photosensitization behavior. Colocalization studies demonstrated the ER-targeting property for complexes **1a** and **1b** that were appended with a tosylamide moiety. Also, the photocytotoxicity of complex **3a** was found to be dependent on the post-treatment incubation time for the conversion to the DNPS-free product **3aP** inside the cells, which enables more efficient photosensitization of cytotoxic $^1O_2$. We anticipate that further modification of the complexes with other biocompatible moieties would lead to the development of new biological reagents for theranostic applications.

Experimental Section

General Information: All solvents were of analytical grade and purified according to standard procedures.[27] Dinitrobenzenesulfonyl chloride was purchased from Alfa. *N*-(2-Aminoethyl)-4-methylbenzenesulfonamide, sodium borohydride, NEM, GSH, GSH ethyl ester, Cys, MTT, 4,4′-dimethyl-2,2′-bipyridine, selenium dioxide, and sodium metabisulfite were purchased from Sigma-Aldrich. Silver trifluoromethanesulfonate, triethylamine, magnesium sulfate, 3-(aminomethyl)pyridine, $Re(CO)_5Br$, phen, Me_4-phen, Ph_2-phen, and DPBF were purchased from Acros. The ligand bpy-CHO,[28] *N*-(2-aminoethyl)-4-methylbenzenesulfonamide,[29] and the rhenium(I) complexes $[Re(N^N)(CO)_3(L)](CF_3SO_3)$ (N^N=Me_4-phen, Ph_2-phen, and phen; L=CH_3CN, pyridine)[17] were prepared according to the literature procedures. All buffer components were of biological grade and used as received. Dulbecco's modified Eagle's medium (DMEM), (PBS), fetal bovine serum (FBS), penicillin/streptomycin, trypsin-EDTA, MitoTracker Deep Red FM, and ER-Tracker Green were purchased from Invitrogen. Autoclaved Milli-Q water was used for the preparation of the aqueous solutions. HeLa cells were obtained from American Type Culture Collection. The growth medium for cell culture contained DMEM mixture with 10 % FBS and 1 % penicillin/streptomycin.

4-*N*-((*p*-Toluenesulfonylamino)ethyl)aminomethyl-4′-methyl-2,2′-bipyridine (bpy-tosylamide): A mixture of bpy-CHO (198 mg, 1 mmol) and *N*-(2-aminoethyl)-4-methylbenzenesulfonamide (214 mg, 1 mmol) in EtOH (20 mL) was heated to reflux under an inert atmosphere of nitrogen for 3 h. The reaction mixture was cooled in an ice-bath, and solid $NaBH_4$ (114 mg, 3 mmol) was slowly added. After stirring for 3 h at room temperature, water (15 mL) was added to quench the reaction and the resulting mixture was extracted with CH_2Cl_2 (20 mL × 3). The combined organic layer was dried over anhydrous $MgSO_4$, filtered, and evaporated under vacuum to give a colorless oil, which was purified by column chromatography on silica gel using CH_2Cl_2/MeOH/NH_4OH (50 : 1 : 0.2 by volume) as the eluent. The solvent was removed under reduced pressure to afford the product as a colorless oil. Yield: 77 mg (55 %). ^{1}H NMR (400 MHz, $CDCl_3$, 298 K, TMS). δ = 8.58 (d, J = 4.8 Hz, 1H, H6 of bpy), 8.51 (d, J = 4.8 Hz, 1H, H6′ of bpy), 8.23 (d, J = 9.1 Hz, 2H, H3 and H3′ of bpy), 7.72 (d, J = 8.1 Hz, 2H, H3 and H5 of phenyl ring), 7.24 (d, J = 8.4 Hz, 2H, H2 and H6 of phenyl ring), 7.14 (dd, J = 8.7 and 4.8 Hz, 2H, H5 and H5′ of bpy), 3.74 (s, 2H, CH_2NH at C4 of bpy), 3.02 (t, J = 5.7 Hz, 2H, CH_2NHSO$_2$), 2.71 (t, J = 5.4 Hz, 2H, NHCH_2), 2.44 (s, 3H, CH_3 on C4′ of bpy), 2.37 (s, 3H, CH_3 on C4 of phenyl ring). MS (ESI, positive-ion mode): m/z 397 $[M+H]^+$.

3-((2,4-Dinitrophenylsulfonyl)aminomethyl)pyridine (py-DNPS): A mixture of 3-(aminomethyl)pyridine (162 mg, 1.5 mmol) and dinitrophenylsulfonyl chloride (398 mg, 1.5 mmol) in dry THF (20 mL) was heated to reflux for 6 h. The mixture was evaporated to dryness under reduced pressure to give a yellow solid. The solid was dissolved in CH_2Cl_2 (20 mL) and washed with H_2O (20 mL × 3). The organic layer was dried over anhydrous $MgSO_4$, filtered, and evaporated to dryness yielding a yellow solid, which was purified by column chromatography on silica gel using CH_2Cl_2/MeOH (50 : 1, *v*/*v*) as the eluent. The solvent was removed under reduced pressure to afford the product as a pale yellow solid. Yield: 210 mg (40 %). ^{1}H NMR (400 MHz, CD_3OD, 298 K, TMS). δ = 8.71 (d, J = 2.2 Hz, 1H, H3 of dinitrophenyl ring), 8.51 (dd, J = 6.3 and 2.2 Hz, 1H, H5 of dinitrophenyl ring), 8.46 (s, 1H, H2 of pyridine), 8.39 (dd, J = 3.4 and 1.4 Hz, 1H, H6 of pyridine), 8.19 (d, J = 6.7 Hz, 1H, H6 of dinitrophenyl ring), 7.81 (d, J = 8.0 Hz, 1H, H4 of pyridine), 7.37–7.33 (m, 1H, H5 of pyridine), 4.40 (s, 2H, CH_2NH). MS (ESI, positive-ion mode): m/z 339 $[M+H]^+$.

[$Re(CO)_3$(bpy-tosylamide)Br]: A mixture of $Re(CO)_5Br$ (217 mg, 0.53 mmol) and bpy-tosylamide (210 mg, 0.53 mmol) in toluene (20 mL) was refluxed under an inert atmosphere of nitrogen for 4 h. The mixture was evaporated to dryness to give a yellow solid. Recrystallization of the solid from CH_2Cl_2/diethyl ether to afford the complex as yellow crystals. Yield: 355 mg (90 %). ^{1}H NMR (300 MHz, CD_3OD, 298 K, TMS). δ = 8.93 (d, J = 5.7 Hz, 1H, H6 of bpy), 8.81 (d, J = 5.7 Hz, 1H, H6′ of bpy), 8.59 (s, 1H, H3 of bpy), 8.49 (s, 1H, H3′ of bpy), 7.76–7.73 (m, 2H, H3 and H5 of phenyl ring), 7.59 (d, J = 5.7 Hz, 1H, H5 of bpy), 7.53 (d, J = 5.7 Hz, 1H, H5′ of bpy), 7.38–7.36 (m, 2H, H2 and H6 of phenyl ring), 3.99 (s, 2H, CH_2NH at C4 of bpy),

3.04 (t, $J=6.0$ Hz, 2H, CH_2NHSO_2), 2.73 (t, $J=6.0$ Hz, 2H, $NHCH_2$), 2.64 (s, 3H, CH_3 at C4′ of bpy), 2.41 (s, 3H, CH_3 at C4 of phenyl ring). IR (KBr) $\tilde{\nu}$/cm^{-1}: 3451 (N–H), 2020 (C≡O), 1902 (C≡O). MS (ESI, positive-ion mode): *m/z* 747 $[M+H]^+$, 668 $[M-Br^-]^+$.

[Re(CO)$_3$(bpy-tosylamide)(CH$_3$CN)](CF$_3$SO$_3$): A mixture of Re(CO)$_3$(bpy-tosylamide)Br (200 mg, 0.27 mmol) and Ag(CF$_3$SO$_3$) (76.8 mg, 0.3 mmol) in CH_3CN (200 mL) was refluxed under an inert atmosphere of nitrogen for 12 h in the dark. The off-white AgBr precipitate was removed by filtration using celite. The filtrate was evaporated under reduced pressure to give a yellow solid. Recrystallization of the solid from CH_2Cl_2/diethyl ether to afford the complex as yellow crystals. Yield: 114 mg (60%). ^{1}H NMR (300 MHz, $CDCl_3$, 298 K, TMS). $\delta=8.85$ (s, 1H, H3 of bpy), 8.79 (d, $J=5.6$ Hz, 1H, H6 of bpy), 8.73 (d, $J=5.6$ Hz, 1H, H6′ of bpy), 8.69 (s, 1H, H3′ of bpy), 7.79–7.76 (m, 2H, H3 and H5 of phenyl ring), 7.5 (d, $J=5.2$ Hz, 1H, H5 of bpy), 7.42 (d, $J=5.2$ Hz, 1H, H5′ of bpy), 7.31–7.28 (m, 2H, H2 and H6 of phenyl ring), 4.21–3.99 (m, 2H, CH_2NH at C4 of bpy), 3.01 (t, $J=1.6$ Hz, 2H, CH_2NHSO_2), 2.86–2.83 (m, 2H, $NHCH_2$), 2.71 (s, 3H, CH_3 at C4′ of bpy), 2.41 (s, 3H, CH_3 at C4 of phenyl ring), 2.23 (s, 3H, CH_3CN). IR (KBr) $\tilde{\nu}$/cm^{-1}: 3451 (N–H), 2020 (C≡O), 1902 (C≡O), 1147 ($CF_3SO_3^-$), 1029 ($CF_3SO_3^-$). MS (ESI, positive-ion mode): *m/z* 707 $[M-CF_3SO_3^-]^+$.

[Re(bpy-tosylamide)(CO)$_3$(py-DNPS)](CF$_3$SO$_3$) (1 a): A mixture of [Re(CO)$_3$(bpy-tosylamide)(CH_3CN)](CF$_3$SO$_3$) (100 mg, 0.14 mmol) and py-DNPS (47 mg, 0.14 mmol) in dry THF (20 mL) was refluxed under an inert atmosphere of nitrogen for 12 h. The mixture was evaporated to dryness under reduced pressure to give an orange solid, which was purified by column chromatography on silica gel using CH_2Cl_2/MeOH (50:1, *v/v*) as the eluent. The solvent was removed under reduced pressure to yield an orange solid. Recrystallization of the solid from CH_2Cl_2/diethyl ether to afford the complex as orange crystals. Yield: 88 mg (63%). ^{1}H NMR (400 MHz, CD_3OD, 298 K, TMS). $\delta=9.19$ (d, $J=5.6$ Hz, 1H, H6 of bpy), 9.13 (d, $J=5.6$ Hz, 1H, H6′ of bpy), 8.76 (d, $J=2.1$ Hz, 1H, H6 of pyridine), 8.65 (s, 1H, H3 of dinitrophenyl ring), 8.56–8.50 (m, 3H, H5 of dinitrophenyl ring and H3 and H3′ of bpy), 8.21 (s, 1H, H2 of pyridine), 8.15 (d, $J=8.6$ Hz, 1H, H6 of dinitrophenyl ring), 7.84–7.82 (m, 2H, H3 and H5 of phenyl ring), 7.71–7.69 (m, 3H, H4 of pyridine and H2 and H6 of phenyl ring), 7.35 (t, $J=7.8$ Hz, 3H, H5 of pyridine and H5 and H5′ of bpy), 4.64 (br, 1H, NH), 4.17 (s, 2H, CH_2NH at C3 of pyridine), 4.04 (s, 2H, CH_2NH at C4 of bpy), 2.97 (t, $J=5.7$ Hz, 2H, CH_2NHSO_2), 2.75 (t, $J=5.8$ H, 2H, $NHCH_2$), 2.64 (s, 3H, CH_3 at C4′ of bpy), 2.42 (s, 3H, CH_3 at C4 of phenyl ring). ^{13}C NMR (150 MHz, CD_3OD, 298 K, TMS), $\delta=195.51$, 155.77, 155.38, 154.59, 152.91, 152.65, 152.62, 150.13, 148.09, 143.42, 138.85, 138.08, 137.47, 137.20, 131.62, 129.57, 129.38, 127.88, 126.72, 126.61, 126.05, 125.51, 120.22, 50.93. 43.01, 42.20, 20.29, 20.01. IR (KBr) $\tilde{\nu}$/cm^{-1}: 3451 (N–H), 2031 (C≡O), 1910 (C≡O), 1145 ($CF_3SO_3^-$), 1029 ($CF_3SO_3^-$). MS (ESI, positive-ion mode): *m/z* 1005 $[M-CF_3SO_3^-]^+$. Anal. Calcd. for $ReC_{37}H_{34}F_3N_8O_{14}S_3\cdot CH_3OH$: C 37.46; H 2.88; N 9.44; found: C 37.59; H 2.62; N 9.17%.

[Re(bpy-tosylamide)(CO)$_3$(pyridine)](CF$_3$SO$_3$) (1 b): The synthetic procedure was similar to that of complex **1 a**, except that pyridine (22 mg, 0.28 mmol) was used instead of py-DNPS. Subsequent recrystallization of the orange solid from CH_2Cl_2/diethyl ether afforded the complex as orange crystals. Yield: 81 mg (76%). ^{1}H NMR (300 MHz, CD_3OD, 298 K, TMS). $\delta=9.22$ (d, $J=5.6$ Hz, 1H, H6 of bpy), 9.15 (d, $J=5.6$ Hz, 1H, H6′ of bpy), 8.63 (s, 1H, H3 of bpy), 8.50 (s, 1H, H3′ of bpy), 8.4 (d, $J=5.1$ Hz, 2H, H2 and H6 of pyridine), 7.93 (t, $J=7.7$ Hz, 1H, H4 of pyridine), 7.83 (d, $J=5.6$ Hz, 1H, H3 of phenyl ring), 7.74–7.71 (m, 3H, H2, H5 and H6 of phenyl ring), 7.41–7.37 (m, 4H, H3 and H5 of pyridine and H5 and H5′ of bpy), 4.03 (s, 2H, CH_2NH at C4 of bpy), 2.97 (t, $J=5.9$ Hz, 2H, CH_2NHSO_2), 2.73 (t, $J=5.9$ Hz, 2H, $NHCH_2$), 2.64 (s, 3H, CH_3 at C4′ of bpy), 2.43 (s, 3H, CH_3 at C4 of phenyl ring). ^{13}C NMR (150 MHz, CD_3OD, 298 K, TMS), $\delta=195.41$, 156.29, 155.83, 155.44, 155.42, 153.01, 152.75, 151.80, 143.42, 139.74, 137.23, 129.38, 129.33, 127.61, 126.63, 1256.56, 125.34, 123.57, 123.30, 121.46, 119.35, 50.89, 42.23, 20.20, 20.02. IR (KBr) $\tilde{\nu}$/cm^{-1}: 3451 (N–H), 2031 (C≡O), 1925 (C≡O), 1148 ($CF_3SO_3^-$), 1030 ($CF_3SO_3^-$). MS (ESI, positive-ion mode): *m/z* 746 $[M-CF_3SO_3^-]^+$. Anal. Calcd. for $ReC_{30}H_{29}F_3N_5O_8S_2\cdot CH_3CN$: C 38.49; H 3.12; N 7.48; found: C 38.55; H 3.36; N 7.37%.

[Re(Me$_4$-phen)(CO)$_3$(py-DNPS)](CF$_3$SO$_3$) (2 a): The synthetic procedure was similar to that of complex **1 a**, except that [Re(Me$_4$-phen)(CO)$_3$(CH_3CN)](CF$_3$SO$_3$) (100 mg, 0.18 mmol) was used instead of [Re(bpy-tosylamide)(CO)$_3$(CH_3CN)](CF$_3$SO$_3$). Subsequent recrystallization of the yellow solid from CH_2Cl_2/diethyl ether afforded the complex as yellow crystals. Yield: 118 mg (78%). ^{1}H NMR (300 MHz, CD_3OD, 298 K, TMS). $\delta=9.43$ (s, 2H, H2 and H9 of Me$_4$-phen), 8.66 (d, $J=2.2$ Hz, 1H, H3 of dinitrophenyl ring), 8.59 (d, $J=5.1$ Hz, 1H, H6 of pyridine), 8.40 (s, 2H, H5 and H6 of Me$_4$-phen), 8.36 (dd, $J=6.4$ and 2.3 Hz, 1H, H5 of dinitrophenyl ring), 8.24 (s, 1H, H2 of pyridine), 7.93 (d, $J=8.6$ Hz, 1H, H4 of pyridine), 7.66 (d, $J=6.7$ Hz, 1H, H6 of dinitrophenyl ring), 7.25–7.20 (m, 1H, H5 of pyridine), 4.06 (s, 2H, CH_2NH at C3 of pyridine), 2.90 (s, 6H, CH_3 at C4 and C7 of Me$_4$-phen), 2.77 (s, 6H, CH_3 at C3 and C8 of Me$_4$-phen). ^{13}C NMR (150 MHz, CD_3OD, 298 K, TMS), $\delta=195.52$, 154.12, 151.57, 150.13, 150.05, 149.01, 148.04, 144.98, 138.73, 138.06, 137.10, 136.43, 131.37, 129.63, 126.49, 125.82, 124.00, 120.13, 42.94, 16.54, 13.98. IR (KBr) $\tilde{\nu}$/cm^{-1}: 3446 (N–H), 2030 (C≡O), 1921 (C≡O), 1160 ($CF_3SO_3^-$), 1031 ($CF_3SO_3^-$). MS (ESI, positive-ion mode): *m/z* 846 $[M-CF_3SO_3^-]^+$. Anal. Calcd. for $ReC_{32}H_{27}F_3N_6O_{12}S_2\cdot H_2O$: C 37.94; H 2.68; N 8.29; found: C 37.96; H 2.87; N 8.34%.

[Re(Ph$_2$-phen)(CO)$_3$(py-DNPS)](CF$_3$SO$_3$) (3 a): The synthetic procedure was similar to that of complex **1 a**, except that [Re(Ph$_2$-phen)(CO)$_3$(CH_3CN)](CF$_3$SO$_3$) (100 mg, 0.15 mmol) was used instead of [Re(bpy-tosylamide)(CO)$_3$(CH_3CN)](CF$_3$SO$_3$). Subsequent recrystallization of the yellow solid from CH_2Cl_2/diethyl ether afforded the complex as yellow crystals. Yield: 109 mg (75%). ^{1}H NMR (300 MHz, CD_3OD, 298 K, TMS). $\delta=9.77$ (d, $J=5.4$ Hz, 2H, H2 and H9 of Ph$_2$-phen), 8.72–8.71 (m, 2H, H6 of pyridine and H3 of dinitrophenyl ring), 8.43 (dd, $J=6.7$ and 2.2 Hz, 1H, H5 of dinitrophenyl ring), 8.37 (s, 1H, H2 of pyridine), 8.21 (s, 2H, H5 and H6 of Ph$_2$-phen), 8.17 (d, $J=5.4$ Hz, 2H, H3 and H8 of Ph$_2$-phen), 8.00 (d, $J=8.6$ Hz, 1H, H4 of pyridine), 7.79–7.64 (m, 11H, H6 of dinitrophenyl ring and C_6H_5 at C4 and C7 of Ph$_2$-phen), 7.37–7.31 (m, 1H, H5 of pyridine), 4.13 (s, 2H, CH_2NH at C3 of pyridine). ^{13}C NMR (150 MHz, CD_3OD, 298 K, TMS), $\delta=195.44$, 191.23, 153.82, 153.02, 150.18, 148.03, 147.15, 138.99, 137.99, 137.46, 135.38, 131.47, 129.80, 129.67, 129.30, 128.87, 127.40, 126.53, 126.10, 126.02, 120.17, 42.92. IR (KBr) $\tilde{\nu}$/cm^{-1}: 3446 (N–H), 2031 (C≡O), 1912 (C≡O), 1158 ($CF_3SO_3^-$), 1029 ($CF_3SO_3^-$). MS (ESI, positive-ion mode): *m/z* 972 $[M-CF_3SO_3^-]^+$. Anal. Calcd. for $ReC_{40}H_{27}F_3N_6O_{12}S_2$: C 44.03; H 2.49; N 7.71; found: C 43.76; H 2.69; N 7.59%.

[Re(phen)(CO)$_3$(py-DNPS)](CF$_3$SO$_3$) (4 a): The synthetic procedure was similar to that of complex **1 a**, except that [Re(phen)(CO)$_3$(CH_3CN)](CF$_3$SO$_3$) (100 mg, 0.20 mmol) was used instead of [Re(bpy-tosylamide)(CO)$_3$(CH_3CN)](CF$_3$SO$_3$). Subsequent recrystallization of the yellow solid from CH_2Cl_2/diethyl ether afforded the complex as yellow crystals. Yield: 114 mg (74%). ^{1}H NMR (300 MHz, $CO(CD_3)_2$, 298 K, TMS). $\delta=9.91$ (d, $J=4.6$ Hz, 2H, H2 and H9 of phen), 9.11 (d, $J=7.4$ Hz, 2H, H4 and H7 of phen), 8.76 (d, $J=2.1$ Hz, 1H, H3 of dinitrophenyl ring), 8.62 (s, 1H, H6 of pyridine), 8.58–8.53 (m, 2H, H2 of pyridine and H5 of dinitrophenyl ring), 8.38–8.31 (m, 4H, H3, H5, H6, and H8 of phen), 8.18 (d, $J=8.6$ Hz, 1H, H4 of pyridine), 7.87 (d, $J=8.1$ Hz, 1H, H6 of dinitrophenyl ring), 7.35–7.31 (m, 1H, H5 of pyridine), 4.3 (s, 2H, CH_2NH at C3 of pyridine). ^{13}C NMR (150 MHz, $CO(CD_3)_2$, 298 K, TMS), $\delta=154.88$, 151.26, 151.22, 150.22, 148.04, 146.47, 140.69, 139.48, 138.15, 137.26, 132.08, 131.40, 128.34, 127.62, 127.13, 126.42, 120.44, 43.37. IR (KBr) $\tilde{\nu}$/cm^{-1}: 3451

(N–H), 2031 (C≡O), 1918 (C≡O), 1144 ($CF_3SO_3^-$), 1026 ($CF_3SO_3^-$). MS (ESI, positive-ion mode): *m/z* 777 [M–$CF_3SO_3^-$]$^+$. Anal. Calcd. for $ReC_{28}H_{19}F_3N_6O_{12}S_2$: C 35.82; H 2.04; N 8.95; found: C 35.84; H 2.06; N 8.71 %.

Physical Measurements and Instrumentation: ^{1}H and ^{13}C NMR spectra were recorded on a Bruker AVANCE III 300, 400, or 600 MHz NMR spectrometer at 298 K. Positive-ion ESI-mass spectra were recorded on an API-3200 Triple-Q MS/MS mass spectrometer at 298 K. IR spectra of samples in potassium bromide (KBr) pellets were obtained using a Thermo Scientific Nicolet iS50 FTIR spectrometer in the range of 4000–400 cm^{-1}. Elemental analyses were carried out on an Elementar Analysensytreme GmbH Vario MICRO elemental analyzer. Electronic absorption and steady-state emission spectra were obtained from an Agilent 8453 diode array spectrophotometer and HORIBA FluoroMax-4 spectrofluorometer, respectively. Luminescence quantum yields were measured by the optically diluted method[30] using degassed [Re(phen)(CO)$_3$(pyridine)](CF$_3$SO$_3$) (Φ_{em} = 0.18, λ_{ex} = 355 nm) as the standard solution.[31] Unless otherwise specified, all the solutions prepared for photophysical studies were degassed with at least four successive freeze-pump-thaw cycles and stored in a 10-cm^3 round-bottomed flask equipped with a sidearm 1-cm fluorescence cuvette and sealed from the atmosphere by a Rotaflo HP6/6 quick-release Teflon stopper. Cyclic voltammetric measurements were carried out using a CH Instruments Electrochemical Workstation CHI 750 A.

Singlet Oxygen ($^1O_2$) Quantum Yield Determination: An aerated DMSO solution (2 mL) containing the rhenium(I) polypyridine complexes and DPBF (10 μM) was introduced to a 1-cm path length quartz cuvette and irradiated at 365 nm. Methylene blue was used as a reference for $^1O_2$ sensitization (Φ_Δ = 0.52).[32] The absorbance of methylene blue and the complexes at 365 nm was adjusted to about 0.15. The absorbance of DPBF at 410 nm was monitored every 10 s. A DMSO solution of DPBF without the complexes was examined to determine its photostability under identical irradiation conditions. The Φ_Δ of the complex was determined by comparing Φ_Δ of rhenium(I)-sensitized DPBF photooxidation to Φ_Δ of methylene blue-sensitized DPBF photooxidation (as reference) and calculated by the following equation:

$$\Phi_\Delta^{sample} = \Phi_\Delta^{MB} \times \frac{m^{sample} \times F^{MB}}{m^{MB} \times F^{sample}}$$

where *m* is the slope of a linear fit of the change in absorbance of DPBF at 410 nm against the irradiation time and *F* is the absorption correlation factor, which is given as $F = 1–10^{-AL}$ (*A* = absorbance at 365 nm and *L* = path length of the cuvette).

ICP-MS Measurements: HeLa cells were grown in a 35-mm tissue culture dish and incubated at 37 °C under a 5 % CO_2 atmosphere for 48 h. After the treatment, the growth medium was replaced by a medium containing the rhenium(I) polypyridine complexes (10 μM) in growth medium/DMSO (99:1, *v/v*) and incubated at 37 °C under a 5 % CO_2 atmosphere. After 2 h incubation, the medium was removed, and the cell layer was washed gently with PBS (1 mL × 3). The cells were trypsinized and harvested with PBS (2 mL). The resultant solution was heated with 65 % HNO_3 (2 mL) at 70 °C for 2 h, cooled to room temperature, and analyzed using an NexION 2000 ICP-MS (PerkinElmer SCIEX Instruments).

Dark Cytotoxicity Assays: HeLa cells were seeded in a 96-well flat-bottomed microplate (≈ 10 000 cells per well) in a growth medium (100 μL) and grown at 37 °C under a 5 % CO_2 atmosphere. After 24 h incubation, the growth medium was replaced by a medium containing the rhenium(I) polypyridine complexes, at concentrations ranging from 10^{-4} to 10^{-7} M in growth medium/DMSO (99:1, *v/v*). Wells containing untreated cells were used as blank controls. The microplate was incubated at 37 °C under a 5 % CO_2 atmosphere for 24 h. Then, MTT in PBS (10 μL, 5 mg mL^{-1}) was added to each well and the microplate was incubated at 37 °C under a 5 % CO_2 atmosphere for 4 h. The growth medium was then removed, and DMSO (200 μL) was added to each well. The microplate was further incubated at 37 °C for 15 min. The absorbance of the solutions at 570 nm was measured with a Powerwave XS MQX200R microplate spectrophotometer (BioTek Instruments Inc., Winooski, VT). The IC_{50} values of the complexes were determined from dose dependence of surviving cells after exposure to the complexes.

Live-cell Confocal Imaging: HeLa cells in growth medium were seeded on sterilized coverslip in 35-mm tissue culture dish and grown at 37 °C under a 5 % CO_2 atmosphere. After 48 h incubation, the growth medium was replaced by a medium containing the rhenium(I) polypyridine complexes (10 μM) in medium/DMSO (99:1, *v/v*) at 37 °C under a 5 % CO_2 atmosphere for 2 h. The growth medium was removed, and the cell layer was washed gently with PBS (1 mL × 3). After that, the coverslip was mounted onto a sterilized glass slide and imaged using a Leica TCS SPE (inverted configuration) confocal microscope and a 63× oil-immersion objective lens. In the co-staining experiments, HeLa cells were incubated with complex **1a** or **1b** (10 μM) for 2 h and then incubated with ER-Tracker Green (1 μM, λ_{ex} = 488 nm, λ_{em} = 500–505 nm) for 20 min. The procedure for HeLa cells treated with complex **3a** was similar to that of complexes **1a** and **1b** except that MitoTracker Deep Red FM (100 nM, λ_{ex} = 635 nm, λ_{em} = 654–674 nm) was used. The colocalization coefficient was determined by the program ImageJ (Version 1.4.3.67).

Intracellular Biothiol-sensing Studies: HeLa cells in growth medium were seeded on sterilized coverslip in two 35-mm tissue culture dishes and grown at 37 °C under a 5 % CO_2 atmosphere. After 48 h, the growth medium in dishes was removed and replaced with fresh medium and medium containing NEM (500 μM), respectively at 37 °C under a 5 % CO_2 atmosphere. After 20 min incubation, the growth medium was removed, and the cell layer was washed gently with PBS (1 mL × 3). The cells were then treated with complex **1a** or **1b** (10 μM) in medium/DMSO (99:1, *v/v*). After incubation for 2 h, the medium was removed, and each cell layer was washed with PBS (1 mL × 3). The coverslip was mounted onto a sterilized glass slide and then imaged using a Leica TCS SPE confocal microscope. The procedure for HeLa cells treated with GSH ethyl ester (1 mM, 2 h) was similar to that of NEM.

Photocytotoxicity Assays: HeLa cells were seeded in two 96-well flat-bottomed microplates (≈10 000 cells per well) in a growth medium (100 μL) and grown at 37 °C under a 5 % CO_2 atmosphere. After 24 h incubation, the growth medium was replaced by medium containing complex **3a** (1 μM) in medium/DMSO (99:1, *v/v*). Wells containing untreated cells were used as blank controls. After incubation at 37 °C under a 5 % CO_2 atmosphere for 2 h, the medium was removed and the cell layer was gently washed with PBS (100 μL) and further incubated in fresh medium for different periods (1, 2, 3, 6, 9, and 12 h) in the dark. Then, the growth medium was replaced by a phenol red-free medium and one of the microplates was illuminated at 365 nm (5 mW cm^{-2}) for 5 min, while the other microplate was kept in dark for 5 min. After irradiation, the medium was removed and fresh growth medium was added, and the cells were incubated in the dark for another 24 h. Then, MTT in PBS (10 μL, 5 mg mL^{-1}) was added to each well, and the microplates were incubated for 4 h. The growth medium was then removed, and DMSO (200 μL) was added to each well. The microplates were further incubated at 37 °C for 15 min. The absorbance of the solution at 570 nm was measured with a

Powerwave XS MQX200R microplate spectrophotometer (BioTek Instruments Inc., Winooski, VT).

ESI-MS Analysis of Cell Extracts: HeLa cells grown for 48 h were incubated with complex **3a** (1 μM) in medium/DMSO (99:1, *v/v*) under a 5% CO_2 atmosphere for 2 h. The stained cells were gently washed with PBS (1 mL×3), and further incubated in the dark for 3 h. Then the medium was removed and the cell layer was washed with PBS (3×1 mL). The cells were trypsinized and harvested with PBS (1 mL×3), and finally lysed by probe sonication with 90 cycles of 10 seconds on, 10 seconds off, at 80% power on an ice bath. The mixture was extracted with CH_2Cl_2 (4 mL×3). The combined organic layer was dried over $MgSO_4$, concentrated in vacuo, and analyzed by ESI-MS.

Acknowledgements

We acknowledge the funding support from the Hong Kong Research Grants Council (Project No. CityU 11300017, CityU 11300318, CityU 11300019, CityU 11302820, and T42-103/16-N), and "Laboratory for Synthetic Chemistry and Chemical Biology" under the Health@InnoHK Program launched by Innovation and Technology Commission, The Government of Hong Kong Special Administrative Region of the People's Republic of China. G.-X. X. acknowledges the receipt of a Postgraduate Studentship administered by City University of Hong Kong.

Conflict of Interest

The authors declare no conflict of interest.

Keywords: Bioimaging probes · Cytotoxicity · Dinitrophenylsulfonamide · Endoplasmic reticulum · Glutathione · Rhenium

[1] a) Y. Tang, D. Lee, J. Wang, G. Li, J. Yu, W. Lin, J. Yoon, *Chem. Soc. Rev.* **2015**, *44*, 5003–5015; b) N. Ballatori, S. M. Krance, S. Notenboom, S. Shi, K. Tieu, C. L. Hammond, *Biol. Chem.* **2009**, *390*, 191–214; c) G. Wu, Y. Fang, S. Yang, J. R. Lupton, N. D. Turner, *J. Nutr.* **2004**, *134*, 489–492; d) J. M. Kim, H. Kim, S. B. Kwon, S. Y. Lee, S.-C. Chung, D.-W. Jeong, B.-M. Min, *Biochem. Biophys. Res. Commun.* **2004**, *325*, 101–108.

[2] a) M. Wei, P. Yin, Y. Shen, L. Zhang, J. Deng, S. Xue, H. Li, B. Guo, Y. Zhang, S. Yao, *Chem. Commun.* **2013**, *49*, 4640–4642; b) J. Zhang, A. Shibata, M. Ito, S. Shuto, Y. Ito, B. Mannervik, H. Abe, R. Morgenstern, *J. Am. Chem. Soc.* **2011**, *133*, 14109–14119; c) H. Maeda, H. Matsuno, M. Ushida, K. Katayama, K. Saeki, N. Itoh, *Angew. Chem. Int. Ed.* **2005**, *44*, 2922–2925; *Angew. Chem.* **2005**, *117*, 2982–2985.

[3] a) L. Niu, Y. Chen, H. Zheng, L. Wu, C. Tung, Q. Yang, *Chem. Soc. Rev.* **2015**, *44*, 6143–6160; b) C. Yin, F. Huo, J. Zhang, R. Martínez-Máñez, Y. Yang, H. Lv, S. Li, *Chem. Soc. Rev.* **2013**, *42*, 6032–6059.

[4] a) G. Yu, X. Zhao, J. Zhou, Z. Mao, X. Huang, Z. Wang, B. Hua, Y. Liu, F. Zhang, Z. He, O. Jacobson, C. Gao, W. Wang, C. Yu, X. Zhu, F. Huang, X. Chen, *J. Am. Chem. Soc.* **2018**, *140*, 8005–8019; b) Y. Wi, H. T. Le, P. Verwilst, K. Sunwoo, S. J. Kim, J. E. Song, H. Y. Yoon, G. Han, J. S. Kim, C. Kang, T. W. Kim, *Chem. Commun.* **2018**, *54*, 8897–8900; c) M. H. Lee, J. H. Han, P.-S. Kwon, S. Bhuniya, J. Y. Kim, J. L. Sessler, C. Kang, J. S. Kim, *J. Am. Chem. Soc.* **2012**, *134*, 1316–1322.

[5] a) K.-X. Teng, L.-Y. Niu, Y.-F. Kang, Q.-Z. Yang, *Chem. Sci.* **2020**, *11*, 9703–9711; b) C. Wang, F. Cao, Y. Ruan, X. Jia, W. Zhen, X. Jiang, *Angew. Chem. Int. Ed.* **2019**, *58*, 9846–9850; *Angew. Chem.* **2019**, *131*, 9951–9955; c) G. Yang, C. Chen, Y. Zhu, Z. Liu, Y. Xue, S. Zhong, C. Wang, Y. Gao, W. Zhang, *ACS Appl. Mater. Interfaces* **2019**, *11*, 44961–44969.

[6] a) S. Monro, K. L. Colon, H. Yin, J. Roque III, P. Konda, S. Gujar, R. P. Thummel, L. Lilge, C. G. Cameron, S. A. McFarland, *Chem. Rev.* **2019**, *119*, 797–828; b) C. Imberti, P. Zhang, H. Huang, P. J. Sadler, *Angew. Chem. Int. Ed.* **2020**, *59*, 61–73; *Angew. Chem.* **2020**, *132*, 61–73; c) J. Shum, P. K.-K. Leung, K. K.-W. Lo, *Inorg. Chem.* **2019**, *58*, 2231–2247.

[7] a) M. Ethirajan, Y. Chen, P. Joshi, R. K. Pandey, *Chem. Soc. Rev.* **2011**, *40*, 340–362; b) B. M. Luby, C. D. Walsh, G. Zheng, *Angew. Chem. Int. Ed.* **2019**, *58*, 2558–2569; *Angew. Chem.* **2019**, *131*, 2580–2591.

[8] a) X. Li, S. Kolemen, J. Yoon, E. U. Akkaya, *Adv. Funct. Mater.* **2017**, *27*, 1604053–1604063; b) H. Fan, G. Yan, Z. Zhao, X. Hu, W. Zhang, H. Liu, X. Fu, T. Fu, X.-B. Zhang, W. Tan, *Angew. Chem. Int. Ed.* **2016**, *55*, 5477–5482; *Angew. Chem.* **2016**, *128*, 5567–5572.

[9] a) A. P. King, J. J. Wilson, *Chem. Soc. Rev.* **2020**, *49*, 8113–8136. b) C. Huang, T. Li, J. Liang, H. Huang, P. Zhang, S. Banerjee, *Coord. Chem. Rev.* **2020**, *408*, 213178–213193; c) A. Raffaello, C. Mammucari, G. Gherardi, R. Rizzuto, *Trends Biochem. Sci.* **2016**, *41*, 1035–1049; d) J. R. Cubillos-Ruiz, S. E. Bettigole, L. H. Glimcher, *Cell* **2017**, *168*, 692–706.

[10] a) M. Wang, R. J. Kaufman, *Nat. Rev. Cancer* **2014**, *14*, 581–597; b) C. Hetz, J. M. Axten, J. B. Patterson, *Nat. Chem. Biol.* **2019**, *15*, 764–775.

[11] a) C. Hwang, A. J. Sinskey, H. F. Lodish, *Science* **1992**, *257*, 1496–1502; b) B. M. Dixon, S. H. D. Heath, R. Kim, J. H. Suh, T. M. Hagen, *Antioxid. Redox Signaling* **2008**, *10*, 963–972.

[12] a) Y. Li, X. Zhang, X. Wan, X. Liu, W. Pan, N. Li, B. Tang, *Adv. Funct. Mater.* **2020**, *30*, 2000532–2000544; b) B. Dong, Y. Lu, N. Zhang, W. Song, W. Lin, *Anal. Chem.* **2019**, *91*, 5513–5516; c) L. Fang, G. Trigiante, R. Crespo-Otero, C. S. Hawes, M. P. Philpott, C. R. Jones, M. Watkinson, *Chem. Sci.* **2019**, *10*, 10881–10887.

[13] a) S. Munro, H. R. B. Pelham, *Cell* **1986**, *46*, 291–300; b) L. C.-C. Lee, A. W.-Y. Tsang, H.-W. Liu, K. K.-W. Lo, *Inorg. Chem.* **2020**, *59*, 14796–14806.

[14] a) K. K.-W. Lo, *Acc. Chem. Res.* **2020**, *53*, 32–44; b) K. K.-W. Lo, K. K.-S. Tso, *Inorg. Chem. Front.* **2015**, *2*, 510–524; c) K. Qiu, Y. Chen, T. W. Rees, L. Ji, H. Chao, *Coord. Chem. Rev.* **2019**, *378*, 66–86.

[15] a) K. K.-S. Tso, H.-W. Liu, K. K.-W. Lo, *J. Inorg. Biochem.* **2017**, *177*, 412–422; b) S. P.-Y. Li, V. M.-W. Yim, J. Shum, K. K.-W. Lo, *Dalton Trans.* **2019**, *48*, 9692–9702; c) Q. Gao, W. Zhang, B. Song, R. Zhang, W. Guo, J. Yuan, *Anal. Chem.* **2017**, *89*, 4517–4524.

[16] a) T. Huang, Q. Yu, S. Liu, K. Y. Zhang, W. Huang, Q. Zhao, *ChemBioChem* **2019**, *20*, 576–586; b) H. Xiang, H. Chen, H. P. Tham, S. Z. F. Phua, J. Liu, Y. Zhao, *ACS Appl. Mater. Interfaces* **2017**, *9*, 27553–27562; c) L. Zeng, S. Kuang, G. Li, C. Jin, L. Ji, H. Chao, *Chem. Commun.* **2017**, *53*, 1977–1980.

[17] a) J. Yang, J. Zhao, Q. Cao, L. Hao, D. Zhou, Z. Gan, L. Ji, Z.-W. Mao, *ACS Appl. Mater. Interfaces* **2017**, *9*, 13900–13912; b) A. M.-H. Yip, J. Shum, H.-W. Liu, H. Zhou, M. Jia, N. Niu, Y. Li, C. Yu, K. K.-W. Lo, *Chem. Eur. J.* **2019**, *25*, 8970–8974.

[18] a) L. C.-C. Lee, P. K.-K. Leung, K. K.-W. Lo, *Dalton Trans.* **2017**, *46*, 16357–16380; b) K. K.-W. Lo, *Acc. Chem. Res.* **2015**, *48*, 2985–2995; c) A. M.-H. Yip, K. K.-W. Lo, *Coor. Chem. Rev.* **2018**, *361*, 138–163. d) J. Shum, P.-Z. Zhang, L. C.-C. Lee, K. K.-W. Lo, *ChemPlusChem* **2020**, *85*, 1374–1378; e) A. W.-T. Choi, K. K.-S. Tso, V. M.-W. Yim, H.-W. Liu, K. K.-W. Lo, *Chem. Commun.* **2015**, *51*, 3442–3445; f) Z. Huang, J. J. Wilson, *Eur. J. Inorg. Chem.* **2021**, *14*, 1312–1324 .

[19] a) A. W.-T. Choi, H.-W. Liu, K. K.-W. Lo, *J. Inorg. Biochem.* **2015**, *148*, 2–10; b) L. Sacksteder, M. Lee, J. N. Demas, B. A. DeGraff, *J. Am. Chem. Soc.* **1993**, *115*, 8230–8238.

[20] a) A. W.-T. Choi, V. M.-W. Yim, H.-W. Liu, K. K.-W. Lo, *Chem. Eur. J.* **2014**, *20*, 9633–9642; b) A. W.-T. Choi, C.-S. Poon, H.-W. Liu, H.-K. Cheng, K. K.-W. Lo, *New J. Chem.* **2013**, *37*, 1711–1719.

[21] C. Jiang, Z. Cheng, Y. Ge, J. Song, J. Zhang, H. Zhang, *Anal. Methods* **2019**, *11*, 3736–3740.

[22] a) X. Jiang, J. Chen, A. Bajić, C. Zhang, X. Song, S. L. Carroll, Z. Cai, M. Tang, M. Xue, N. Cheng, C. P. Schaaf, F. Li, K. R. MacKenzie, A. C. M. Ferreon, F. Xia, M. Wang, M. Maletić-Savatić, J. Wang, *Nat. Commun.* **2017**, *8*, 16087–16098; b) J. Sun, X. Cai, C. Wang, K. Du, W. Chen, F. Feng, S. Wang, *J. Am. Chem. Soc.* **2021**, *143*, 868–878; c) J. Liu, Y. Sun, Y. Huo, H. Zhang, L. Wang, P. Zhang, D. Song, Y. Shi, W. Guo, *J. Am. Chem.* **2014**, *136*, 574–577.

[23] a) K. Y. Zhang, K. K.-W. Lo, *Inorg. Chem.* **2009**, *48*, 6011–6025; b) R. Chaudhary, K. Roy, R. K. Kanwar, R. N. Veedu, S. Krishnakumar, C. H. A. Cheung, A. K. Verma, J. R. Kanwar, *Aust. J. Chem.* **2016**, *69*, 1108–1116; c) C. Li, Y. Liu, Y. Wu, Y. Sun, F. Li, *Biomaterials* **2013**, *34*, 1223–1234; d) H. Kasai, K. Inoue, K. Imamura, C. Yuvienco, J. K. Montclare, S. Yamano, *J. NanoBiotechnology* **2019**, *17*, 1–14.

[24] a) C. C. Konkankit, A. P. King, K. M. Knopf, T. L. Southard, J. J. Wilson, *ACS Med. Chem. Lett.* **2019**, *10*, 822–827; b) F.-X. Wang, J.-H. Liang, H. Zhang,

Z.-H. Wang, Q. Wan, C.-P. Tan, L.-N. Ji, Z.-W. Mao, *ACS Appl. Mater. Interfaces* **2019**, *11*, 13123–13133; c) K. Y. Zhang, K. K.-S. Tso, M.-W. Louie, H.-W. Liu, K. K.-W. Lo, *Organometallics* **2013**, *32*, 5098–5102.
[25] a) L. D. Ramos, H. M. da Cruz, K. P. M. Frin, *Photochem. Photobiol. Sci.* **2017**, *16*, 459–466; b) F. Ragone, H. H. M. Saavedra, P. M. D. Gara, G. T. Ruiz, E. Wolcan, *J. Phys. Chem. A* **2013**, *117*, 4428–4435; c) S. C. Marker, S. N. MacMillan, W. R. Zipfel, Z. Li, P. C. Ford, J. J. Wilson, *Inorg. Chem.* **2018**, *57*, 1311–1331.
[26] P. K.-K. Leung, K. K.-W. Lo, *Chem. Commun.* **2020**, *56*, 6074–6077.
[27] D. D. Perrin, W. L. F. Armarego, *Purification of Laboratory Chemicals*, Elsevier, Oxford, U. K., **2009**.
[28] B. M. Peek, G. T. Ross, S. W. Edwards, G. J. Meyer, T. J. Meyer, B. W. Erickson, *Int. J. Pept. Protein Res.* **1991**, *38*, 114–123.
[29] S. Li, D. Zhou, Y. Li, H. Liu, P. Wu, J. Ou-Yang, W. Jiang, C. Li, *ACS Sens.* **2018**, *3*, 2311–2319.
[30] J. N. Demas, G. A. Crosby, *J. Phys. Chem.* **1971**, *75*, 991–1024.
[31] L. Wallance, D. P. Rillema, *Inorg. Chem.* **1993**, *32*, 3836–3843.
[32] M. C. DeRosa, R. J. Crutchley, *Coord. Chem. Rev.* **2002**, *233–234*, 351–571.

Manuscript received: April 30, 2021
Revised manuscript received: June 9, 2021
Accepted manuscript online: June 15, 2021